

Determination of Local Short-Range Order in TiVNbHf(Al)

Michael Xu,¹ Shaolou Wei,¹ Cemal C. Tasan,¹ and James M. LeBeau¹

Department of Materials Science and Engineering, Massachusetts Institute of Technology, Cambridge, MA 02139

(*Corresponding author, Email: lebeau@mit.edu)

(Dated: 8 February 2023)

The presence of short-range chemical order can be a key factor in determining the mechanical behavior of metals, but directly and unambiguously determining its distribution in complex concentrated alloy systems can be challenging. Here, we directly identify and quantify chemical order in the globally single phase BCC-TiVNbHf(Al) system using aberration corrected scanning transmission electron microscopy (STEM) paired with spatial statistics methods. To overcome the difficulties of short-range order (SRO) quantification with STEM when the components of an alloy exhibit large atomic number differences and near equiatomic ratios, “null hypothesis” tests are used to separate experiment from a random chemical distribution. Experiment is found to deviate from both the case of an ideal random solid solution and a fully ordered structure with statistical significance. We also identify local chemical order in TiVNbHf and confirm and quantify the enhancement of SRO with the addition of Al. These results provide insights into local chemical order in the promising TiVNbHf(Al) refractory alloys while highlighting the utility of spatial statistics in characterizing nanoscale SRO in compositionally complex systems.

Refractory high entropy alloys (RHEAs), composed of multi-principal refractory components, have garnered significant interest due to their high-temperature performance and potential for hierarchical control of constituent phases and microstructures at a variety of length scales¹. Notably, the presence and manipulation of ordered precipitates – down to the nanoscale – improves ductility and performance of several alloys in this design space^{2,3}. Of particular interest are RHEAs based on Ti, V, Nb, and Hf that have been shown to exhibit high strength and ductility at room temperature with the potential for local chemical order^{4–6}. In these and similar alloys, the existence of local chemical fluctuations, either through ordering or clustering, have been predicted and connected to the favorable mechanical response seen in these systems^{6,7}. Such local fluctuations and associated increased yield strength are thought to arise from the varying constituent elements’ chemical affinities and site preferences, specifically among Ti, Nb, and Hf⁸.

Control of the local order in Ti- and Nb-containing RHEAs has been enabled through the addition of Al, where properties including strength, ductility, density, and oxidation resistance have been maintained or improved^{1,9–15}. In an AlTiNbZrW system, for example, a microstructure consisting of B2 nanoprecipitates in a BCC matrix has been attributed to exceptional room temperature and high temperature specific yield strength and plasticity¹⁵. Similarly, Al-modulation has been shown to provide a systematic increase in yield strength and elongation in an AlNbTiZr system due to dislocation interactions with SRO¹⁴. Moreover, the elastic response of these systems has been suggested to depend on local thermodynamically stable configurations of order and disorder¹⁶. While controlling the formation of order in refractory high entropy alloys provides a promising route for microstructural and property engineering, direct, nanoscale investigations of these phenomena are required to provide new insights and model validation.

While comparing the binary compound formation enthalpies and mixing enthalpies across Ti, V, Nb, and Hf suggests that local short-range order (SRO) should be possible

($\Delta H_f^{binary} \approx -5$ to 4 kJ/mol and $\Delta H_{mix} \approx -2$ to 4 kJ/mol)^{17,18}, this has not been directly confirmed to the best of our knowledge. Moreover, characterizing SRO in these systems using techniques including STEM, X-ray diffraction, and neutron diffraction remains a challenge in part due to the presence of extremely local chemical fluctuations as well as significant differences in atomic number¹⁹. To complicate matters, the stability of B2 SRO/LRO has been suggested to arise due to a strong sublattice site disorder from the multi-component nature of these alloys²⁰, raising the question of how to differentiate order from disorder with confidence.

In this work, we show the presence of extremely local (<2 nm) SRO in the refractory high entropy Ti₃₈V₁₅Nb₂₃Hf₂₄ alloy using a combination of atomic resolution STEM imaging and spatial statistics methods²¹. To do so, we apply the Moran’s I statistic, a two-dimensional autocorrelation analogous to the Warren-Cowley parameter. By establishing upper and lower “bounds” on the measurements obtained from atomic resolution STEM, local random chemical fluctuations in a ideal disordered random solid solution (RSS) are shown to be inconsistent with experiment. Specifically, the non-random, sublattice-based order between (TiV) and (NbHf) is found to be consistent with predicted site occupancies and bond preferences²⁰. Finally, we show that the addition of Al leads to a small but statistically significant enhancement of short-range ordering. Overall, the results of this study demonstrate the power of STEM to determine and quantify SRO at extremely short length scales in chemically complex systems.

Details of the base Ti₃₈V₁₅Nb₂₃Hf₂₄ and Al-addition (Ti₃₈V₁₅Nb₂₃Hf₂₄)₉₅Al₅ alloy fabrication and characterization are included in Supplementary Information (also see Ref. 5). Figure 1 shows the integrated synchrotron X-ray diffraction profiles for the base and the Al-addition RHEAs. Both profiles correspond only to single phase BCC, even though the addition of Al is predicted to form distinct, long-range ordered phases. Moreover, through Rietveld refinement, Al addition is found to reduce the lattice parameter by 0.5% (3.304 Å for the Al-addition alloy compared with 3.323 Å for

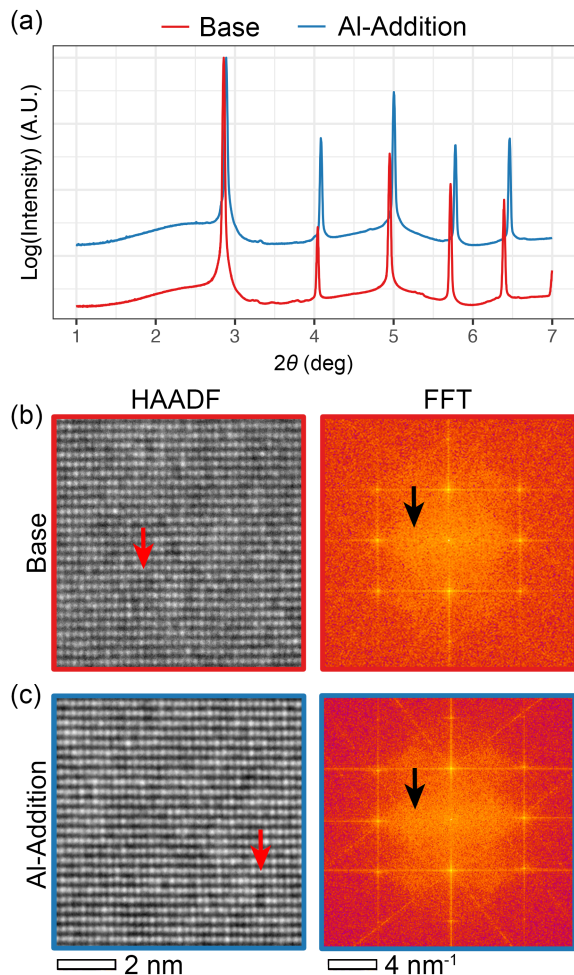


FIG. 1. (a) Synchrotron X-ray diffraction profiles for the base and Al-addition alloys. HAADF STEM image and corresponding Fourier transform of the (b) base and (c) Al-addition alloys, showing diffuse structure. Some regions with local bright /dim atomic planes are indicated.

the base alloy⁵). While total X-ray or neutron scattering can reveal SRO in these systems, these techniques provide a global average of the local structure^{22–24}. For unambiguous direct observation and comparison of SRO, especially in the case of diffuse or extremely short-range order, a more localized probe is needed^{25–27}.

Imaging both alloys at the atomic scale with HAADF STEM (Figure 1b-c) shows strong contrast variation between neighboring atom columns, with many bright and dim bands appearing on $\{002\}$ -type planes (see arrows in the figure). Based on the corresponding Fourier transforms, no discrete superlattice reflections are present, indicating the lack of long-range ordered structure. This is in agreement with synchrotron diffraction measurements. The presence of significant diffuse intensity between the 002 Bragg spots (indicated in the FFTs in Figure 1b-c), however, suggests that local ordering exists on $\{002\}$ -type planes, or B2-type SRO, and originates from bright/dim neighboring planes in the HAADF STEM images.

To visualize the atom column intensity variation more

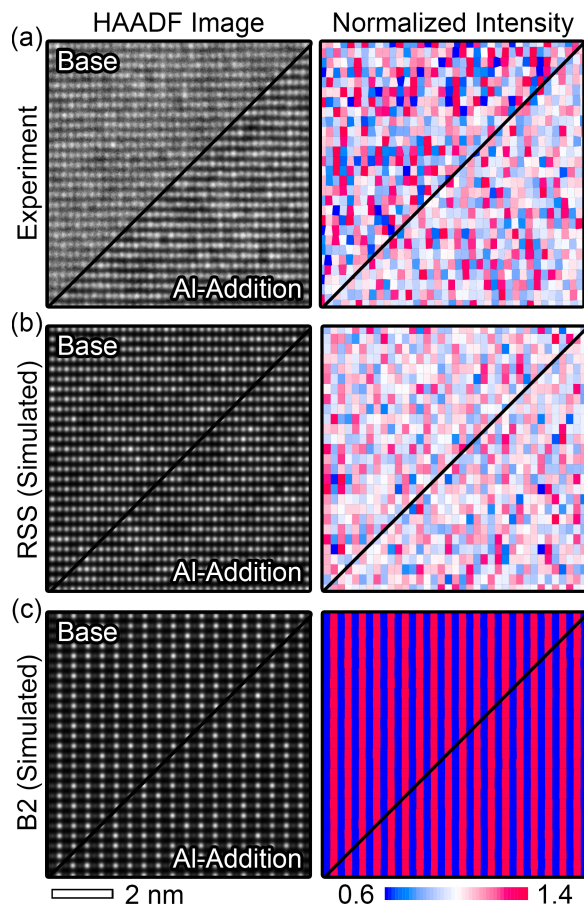


FIG. 2. HAADF STEM images and normalized intensity maps from (a) experiment, (b) ideal random solid solution STEM image simulation, and (c) ideal B2 order STEM image simulation for the base and Al-addition alloys.

clearly, each atom column is normalized with respect to the average of its six nearest neighbor atom columns on adjacent $\{002\}$ planes. The resulting normalized intensity map, shown in Figure 2a, highlights differences in atom column atomic number contrast²⁵. This alternating intensity is present across both the base and Al-addition alloys, and at first glance suggests short-range B2-like ordering. Further, a correlated intensity (order metric²⁸) map highlights regions of order yields hotspots of similar size and shape (Supplementary Information Figure S1). Based on the binary compound formation enthalpies (see Ref. 17), this ordering between higher and lower atomic number elements appears to be consistent, yet the magnitudes of these enthalpies is small in comparison to other binary compound formers, including Al-containing compounds. An additional issue is apparent from comparing the normalized intensity maps of the base and Al-addition alloys. Less intense variation is seen in the Al-addition alloy, which would conventionally suggest weakened ordering²⁵ contrary to the effect of Al in forming ordered intermetallics and SRO in similar systems^{1,14,17}.

Determining the origin of the discrepancies with atomic resolution imaging is complicated by the projection-limited

aspect of STEM. While hypothesis testing has been used to confidently identify SRO in systems with minimal atomic number variation, such as NiFeCrCo²⁵, the wide atomic number difference between the elements in the alloys studied here introduce other issues. This is demonstrated using STEM image simulations of randomized structures with the experimental alloy compositions (Figure 2b). The results are visually very similar to the atom column contrast, normalized intensity maps, and correlated intensity (order metric) maps (see Supplementary Information Figure S1) obtained from experiment. Further, the histograms of order metric (correlated intensity, Supplementary Information Figure S2) show only slight deviation between simulated images and experiment for the Al-addition alloy.

Apparent ordering of atom column intensities is present even for the random structures based on STEM imaging. This can be explained by the presence of atoms with large atomic number differences and similar atomic percent, where the local random compositional fluctuations lead to a wide variation in contrast. Thus, there is an intrinsic amount of variation among atom column intensities purely due to the nature of STEM imaging, which introduces SRO-like contrast to these images. Depending on the composition of the alloy, differing amounts of “pseudo-SRO” will be present even for ideal disordered structures. This issue thus presents a significant challenge in identifying and quantifying real SRO using direct STEM imaging.

By “bounding” the limits of SRO using randomized and fully-ordered structures, however, statistical comparisons can be made to confidently interpret SRO from experiment and reconcile discrepancies in predicted order/disorder²¹. Using the bulk compositions as constraints, STEM images of seven random (A2) and seven fully B2-ordered structures for both the base and Al-addition alloys are simulated using the multislice method²⁹. For the random structures, elements are randomly dispersed throughout the entire BCC <110>-oriented and thickness-matched supercells to be consistent with the bulk composition (Figure 3a). In the case of fully B2-ordered structures, Al is randomly dispersed throughout the supercell, where Ti/V and Nb/Hf are randomly partitioned onto separate sublattices, with the excess Ti/V dispersed onto the other sublattice (Figure 3a).

To verify ordering in the simulated supercells, the Warren-Cowley pair correlations are used, given by

$$\alpha_{ij}^{mn} = 1 - \frac{P(i^m | j^n)}{c_i} \quad (1)$$

where $P(i^m | j^n)$ is the conditional probability of finding an i atom at site m given a j atom at site n , and c_i is the overall concentration of i . Symmetry of the lattice reduces the independent parameters to a function of neighbor shell k , giving α_{ij}^k , which is evaluated to the second near neighbor shell^{30,31}. The resulting pair correlations confirm the ordered and disordered nature of B2 and random structures, respectively (Figure 3b-c).

To quantitatively measure order and uncover differences between simulated and experimental STEM images, a neighbor-based Moran’s I statistic approach is applied, with further de-

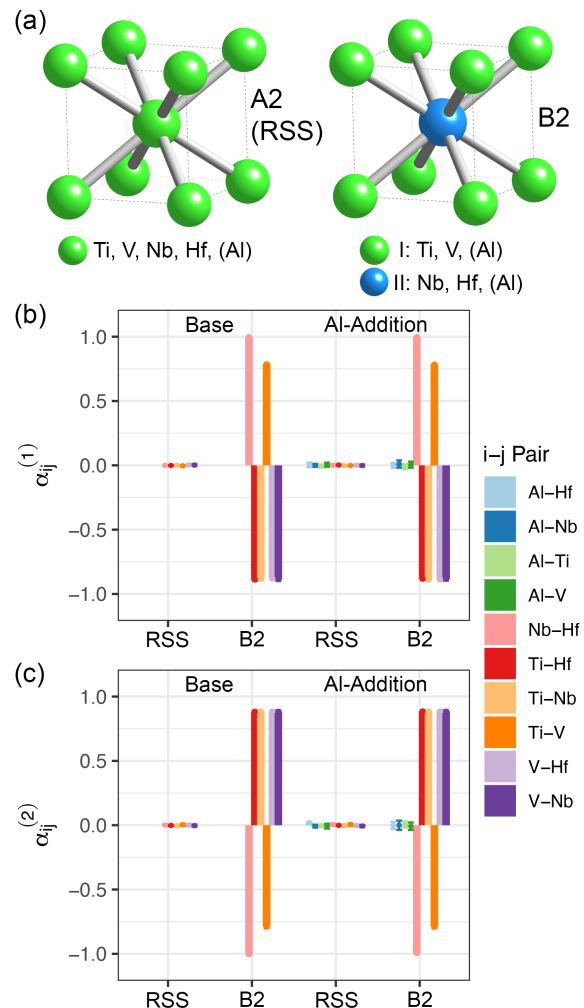


FIG. 3. (a) Schematic of ideal random (A2) and ordered (B2) structures with respective sublattice site occupancies. (b) First and (c) second near-neighbor Warren-Cowley pair correlations for the ideal random and ordered base and Al-addition alloy structures, averaged across seven supercells each.

tails provided in Ref. 21. Essentially, this metric quantifies the similarity of a feature with respect to near neighbor shells and allows for the tendency and degree of order to be determined. To account for differences in the limited field-of-view and the number of sampled atom columns, sub-regions of several experimental datasets are sampled randomly to match the simulation field-of-view, and the Moran’s I ordering values are calculated individually to provide the standard deviations (error bars in Figure 4).

For simulations of the base and Al containing alloys, significant $\{002\}$ order is seen based on the pattern and magnitude of the Moran’s I values across the five nearest neighbors in projection (Figure 4a-b). In the fully ordered case, the Moran’s I values are near ± 1 and display a pattern consistent with complete and long-range B2 order. Unexpectedly, in the random case, a pattern corresponding to $\{002\}$ order is still present, confirming the local order-like features seen from the normalized intensity maps. Thus, when atoms

of large atomic number differences with near equiatomic ratios are being investigated with HAADF STEM, care must be taken when making conclusions about the nature of SRO.

The simulated fully ordered and disordered structures also establish a baseline with which STEM measurements of order cannot be distinguished from randomized site occupancy. In other words, Moran's I ordering "greater" than that of the random case is thus required to separate fully disordered structures from ones with true SRO. The experimental results from the base and Al-addition TiVNbHf alloys satisfy this criterion – the Moran's I ordering values are greater than the ideal disordered structures at varying neighbor shells. Moreover, the values are between the random and fully B2 configurations. This is expected for SRO, where the random and long-range ordered structures bound the experimental Moran's I autocorrelations. The error bars (standard deviations) of the Moran's I measured across individual simulations or sub-regions are non-overlapping as well, further suggesting the presence of non-random B2 SRO.

To confirm the statistical significance of differences in ordering between simulated structures and experiment, the Moran's I scatter plots for each neighbor shell, from which the Moran's I values are calculated, are compared using linear regression and least-squares means³². The relationship between normalized intensity and alloy composition is shown to be significant in determining near-neighbor normalized intensity, or the degree of correlated local (neighbor) order. For the base alloy, the intensity pattern found in the STEM images is distinct from random structures, with enhanced B2-like order up to the second near neighbor shell (Figure 4a), while in the Al containing alloy, ordering is statistically distinct up to the fifth near neighbor shell (Figure 4b).

The increase in the degree and spatial extent of SRO in the Al containing alloy is verified by comparing its Moran's I values to those of the base alloy from experiment (Figure 4c). At each neighbor shell, the Moran's I linear fits are statistically distinct between the two compositions at a high significance threshold ($p < 0.0001$), discounting the null hypothesis of no difference between the two linear regressions. Further, the larger magnitude slopes of the Moran's I fits for the Al-addition alloy indicate greater B2-like order (Figure 4d). Thus, at the local level and prior to any secondary phases, Al-addition is shown to enhance SRO formation in TiVNbHf(Al). The correlation length of order in the Al-addition alloy also increases to the fifth nearest neighbor shell in comparison with the base composition, validating the subtle increase in SRO domain radius from 0.53 nm to 0.64 nm estimated from the correlated intensity maps (Supplementary Information Figure S3). Moreover, the enhancement of SRO by Al modulation is consistent with the binary compound formation enthalpies of the given alloy components as well as Al-containing ordered phases in other refractory systems^{1,14,17}.

In conclusion, local random chemical fluctuations in a near-equiatomic multicomponent alloy combined with the nature of HAADF STEM imaging can produce image intensity variations that resemble SRO. To overcome these challenges, fully disordered and ordered supercells can be used to simulate STEM images, with resulting spatial analysis establishing

bounds for the experimental results. Armed with these metrics, the results from experiment confirm the presence of local chemical order in TiVNbHf and provide further insights into enthalpy-dependent bond preferences in these systems. Further, the addition of Al is shown to enhance SRO formation at the local level, offering a route to property enhancement through microstructural control. Future work can build on these results by using the approach to provide quantitative metrics of extremely short-range order to connect to the properties of RHEAs and other compositionally complex systems.

ACKNOWLEDGMENTS

Synchrotron X-ray diffraction measurements were carried out at beamline 11ID-C at the Argonne National Laboratory, Chicago, U.S.A., with the kind support of Dr. Andrey Yakovenko. We acknowledge support for this work from the National Science Foundation (CMMI-1922206). This work made use of the MIT.nano Characterization Facilities.

DATA AVAILABILITY STATEMENT

The data that support the findings of this study are available from the corresponding author upon reasonable request.

- ¹O. N. Senkov, D. B. Miracle, K. J. Chaput, and J.-P. Couzinie, "Development and exploration of refractory high entropy alloys—A review," *Journal of Materials Research* **33**, 3092–3128 (2018).
- ²O. Senkov, J. Jensen, A. Pilchak, D. Miracle, and H. Fraser, "Compositional variation effects on the microstructure and properties of a refractory high-entropy superalloy AlMo0.5NbTa0.5TiZr," *Materials & Design* **139**, 498–511 (2018).
- ³V. Soni, B. Gwalani, T. Alam, S. Dasari, Y. Zheng, O. Senkov, D. Miracle, and R. Banerjee, "Phase inversion in a two-phase, BCC+B2, refractory high entropy alloy," *Acta Materialia* **185**, 89–97 (2020).
- ⁴Y. Wu, Y. Cai, T. Wang, J. Si, J. Zhu, Y. Wang, and X. Hui, "A refractory Hf25Nb25Ti25Zr25 high-entropy alloy with excellent structural stability and tensile properties," *Materials Letters* **130**, 277–280 (2014).
- ⁵S. Wei, S. J. Kim, J. Kang, Y. Zhang, Y. Zhang, T. Furuhashi, E. S. Park, and C. C. Tasan, "Natural-mixing guided design of refractory high-entropy alloys with as-cast tensile ductility," *Nature Materials* **19**, 1175–1181 (2020).
- ⁶Y. Bu, Y. Wu, Z. Lei, X. Yuan, H. Wu, X. Feng, J. Liu, J. Ding, Y. Lu, H. Wang, Z. Lu, and W. Yang, "Local chemical fluctuation mediated ductility in body-centered-cubic high-entropy alloys," *Materials Today* **46**, 28–34 (2021).
- ⁷Z. An, S. Mao, T. Yang, C. T. Liu, B. Zhang, E. Ma, H. Zhou, Z. Zhang, L. Wang, and X. Han, "Spinodal-modulated solid solution delivers a strong and ductile refractory high-entropy alloy," *Materials Horizons* **8**, 948–955 (2020).
- ⁸K. Xun, B. Zhang, Q. Wang, Z. Zhang, J. Ding, and E. Ma, "Local chemical inhomogeneities in TiZrNb-based refractory high-entropy alloys," *Journal of Materials Science & Technology* **135**, 221–230 (2023).
- ⁹O. N. Senkov, C. Woodward, and D. B. Miracle, "Microstructure and Properties of Aluminum-Containing Refractory High-Entropy Alloys," *JOM* **66**, 2030–2042 (2014).
- ¹⁰O. Senkov, S. Senkova, and C. Woodward, "Effect of aluminum on the microstructure and properties of two refractory high-entropy alloys," *Acta Materialia* **68**, 214–228 (2014).
- ¹¹Y. Wu and D. L. Irving, "Prediction of chemical ordering in refractory high-entropy superalloys," *Applied Physics Letters* **119**, 111901 (2021).
- ¹²X. Liu, Z. Bai, X. Ding, J. Yao, L. Wang, Y. Su, Z. Fan, and J. Guo, "A novel light-weight refractory high-entropy alloy with high specific strength and intrinsic deformability," *Materials Letters* **287**, 129255 (2020).

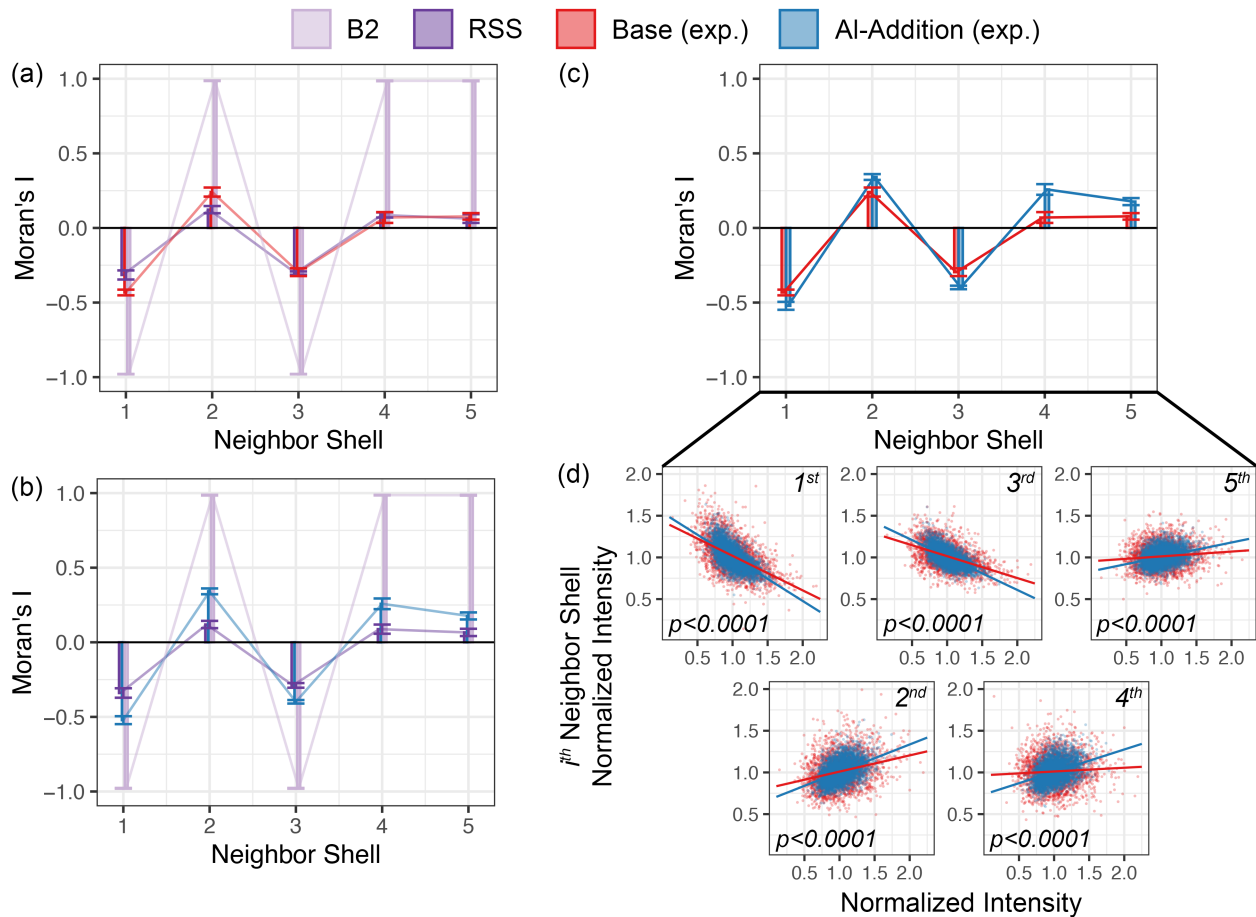


FIG. 4. Bounded Moran's I values across five near-neighbor shells calculated from the normalized intensity STEM image maps for the (a) base alloy and (b) Al-addition alloy. (c) Comparison of Moran's I values between base and Al-addition alloys, with (d) Moran's I scatter plots and corresponding statistical significance at each neighbor shell.

- ¹³X. Zhu, N. Gao, Z. Bai, K. Wang, J. Yao, Z. Fan, Z. Wang, and X. Liu, "Phase stability of a light-weight AlNb₂TiV refractory high-entropy alloy at high temperature," *Materials Letters* **325**, 132897 (2022).
- ¹⁴N. Yurchenko, E. Panina, A. Tojibaev, S. Zherebtsov, and N. Stepanov, "Overcoming the strength-ductility trade-off in refractory medium-entropy alloys via controlled B2 ordering," *Materials Research Letters* **10**, 813–823 (2022).
- ¹⁵M. A. Khan, T.-L. Wang, C. Feng, H. Sun, B. Wang, M. Hamza, G. yasin, M. A. Afifi, and W.-B. Liao, "A superb mechanical behavior of newly developed lightweight and ductile Al_{0.5}Ti₂Nb₁Zr₁W_x refractory high entropy alloy via nano-precipitates and dislocations induced-deformation," *Materials & Design* **222**, 111034 (2022).
- ¹⁶S. Qiu, S.-M. Chen, N. Naihua, J. Zhou, Q.-M. Hu, and Z. Sun, "Structural stability and mechanical properties of b2 ordered refractory alnbtivr high entropy alloys," *Journal of Alloys and Compounds* **886**, 161289 (2021).
- ¹⁷M. C. Tropicovsky, J. R. Morris, P. R. C. Kent, A. R. Lupini, and G. M. Stocks, "Criteria for Predicting the Formation of Single-Phase High-Entropy Alloys," *Physical Review X* **5**, 011041 (2015).
- ¹⁸A. Takeuchi and A. Inoue, "Classification of bulk metallic glasses by atomic size difference, heat of mixing and period of constituent elements and its application to characterization of the main alloying element," *Materials Transactions* **46**, 2817–2829 (2005).
- ¹⁹H. Chen, A. Kauffmann, S. Seils, T. Boll, C. Liebscher, I. Harding, K. Kumar, D. Szabó, S. Schlabach, S. Kauffmann-Weiss, F. Müller, B. Gorr, H.-J. Christ, and M. Heilmaier, "Crystallographic ordering in a series of al-containing refractory high entropy alloys ta–nb–mo–cr–ti–al," *Acta Materialia* **176**, 123–133 (2019).
- ²⁰F. Körmann, T. Kostuchenko, A. Shapeev, and J. Neugebauer, "B2 ordering in body-centered-cubic AlNbTiV refractory high-entropy alloys," *Physical Review Materials* **5**, 053803 (2021).
- ²¹M. Xu, A. Kumar, and J. M. LeBeau, "Correlating local chemical and structural order using Geographic Information Systems-based spatial statistics," *Ultramicroscopy* **243**, 113642 (2023).
- ²²P. A. Lee, P. H. Citrin, P. Eisenberger, and B. M. Kincaid, "Extended x-ray absorption fine structure—its strengths and limitations as a structural tool," *Reviews of Modern Physics* **53**, 769–806 (1981).
- ²³Y. Wu, F. Zhang, X. Yuan, H. Huang, X. Wen, Y. Wang, M. Zhang, H. Wu, X. Liu, H. Wang, S. Jiang, and Z. Lu, "Short-range ordering and its effects on mechanical properties of high-entropy alloys," *Journal of Materials Science & Technology* **62**, 214–220 (2021).
- ²⁴J. L. Hart, A. C. Lang, Y. Li, S. Shahrezaei, D. D. Alix-Williams, M. L. Falk, S. N. Mathaudhu, A. I. Frenkel, and M. L. Taheri, "Revealing Local Order via High Energy EELS," *Materials Today Nano*, 100298 (2022).
- ²⁵C. Niu, A. J. Zaddach, A. A. Oni, X. Sang, J. W. Hurt, J. M. LeBeau, C. C. Koch, and D. L. Irving, "Spin-driven ordering of cr in the equiatomic high entropy alloy nifecrco," *Applied Physics Letters* **106**, 161906 (2015).
- ²⁶R. Zhang, S. Zhao, C. Ophus, Y. Deng, S. J. Vachhani, B. Ozdol, R. Traylor, K. C. Bustillo, J. W. Morris, D. C. Chrzan, M. Asta, and A. M. Minor, "Direct imaging of short-range order and its impact on deformation in ti-6al," *Science Advances* **5**, eaax2799 (2019).
- ²⁷R. Zhang, S. Zhao, J. Ding, Y. Chong, T. Jia, C. Ophus, M. Asta, R. O. Ritchie, and A. M. Minor, "Short-range order and its impact on the crconi medium-entropy alloy," *Nature* **581**, 283–287 (2020).

- ²⁸A. Kumar, J. N. Baker, P. C. Bowes, M. J. Cabral, S. Zhang, E. C. Dickey, D. L. Irving, and J. M. LeBeau, "Atomic-resolution electron microscopy of nanoscale local structure in lead-based relaxor ferroelectrics," *Nature Materials* **20**, 62–67 (2021).
- ²⁹E. J. Kirkland, R. F. Loane, and J. Silcox, "Simulation of annular dark field stem images using a modified multislice method," *Ultramicroscopy* **23**, 77–96 (1987).
- ³⁰J. M. Cowley, "An Approximate Theory of Order in Alloys," *Physical Review* **77**, 669–675 (1950).
- ³¹J. Cowley, "Short-Range Ordering in Crystals," *Advances in High Temperature Chemistry* **3**, 35–85 (1971).
- ³²R. V. Lenth, "Least-Squares Means: The R Package lsmeans," *Journal of Statistical Software* **69** (2016), 10.18637/jss.v069.i01.